



**HAL**  
open science

# Time Reversed Absorbing Condition in the Partial Aperture Case

Franck Assous, Marie Kray, Frédéric Nataf

► **To cite this version:**

Franck Assous, Marie Kray, Frédéric Nataf. Time Reversed Absorbing Condition in the Partial Aperture Case. Wave Motion, 2012, 49 (7), pp.617-631. 10.1016/j.wavemoti.2012.03.006 . hal-00581291

**HAL Id: hal-00581291**

**<https://hal.science/hal-00581291>**

Submitted on 30 Mar 2011

**HAL** is a multi-disciplinary open access archive for the deposit and dissemination of scientific research documents, whether they are published or not. The documents may come from teaching and research institutions in France or abroad, or from public or private research centers.

L'archive ouverte pluridisciplinaire **HAL**, est destinée au dépôt et à la diffusion de documents scientifiques de niveau recherche, publiés ou non, émanant des établissements d'enseignement et de recherche français ou étrangers, des laboratoires publics ou privés.

# Time Reversed Absorbing Condition in the Partial Aperture Case

F. Assous\*, M. Kray†, F. Nataf†

## Abstract

The time-reversed absorbing conditions (*TRAC*) method introduced in [AKNT10, AKNT] enables one to “recreate the past” without knowing the source which has emitted the signals that are back-propagated. It has been applied to inverse problems for the reduction of the computational domain size and for the determination, from boundary measurements, of the location and volume of an unknown inclusion. The method does not rely on any *a priori* knowledge of the physical properties of the inclusion. The aim of this paper is to extend the *TRAC* method to the partial aperture configuration and to discrete receivers with various spacing. In particular the *TRAC* method is applied to the differentiation between a single inclusion and a two close inclusion case. The results are fairly insensitive to noise in the data.

## Contents

<b>1</b>	<b>Introduction</b>	<b>1</b>
<b>2</b>	<b>Principle of the TRAC method</b>	<b>2</b>
<b>3</b>	<b>Recreate the past</b>	<b>5</b>
<b>4</b>	<b>Inverse problem</b>	<b>6</b>
4.1	Criteria . . . . .	9
4.1.1	Final time criterion . . . . .	9
4.1.2	Absorbing boundary condition criterion . . . . .	9
4.1.3	Cross correlation criterion . . . . .	10
4.2	Test cases : numerical results . . . . .	10
4.2.1	One inclusion . . . . .	11
4.2.2	One inclusion vs. two inclusions . . . . .	11
<b>5</b>	<b>Conclusion</b>	<b>19</b>

## 1 Introduction

Time reversal is a subject of very active research. The principle is to take advantage of the reversibility of wave propagation phenomena, for example in acoustics or electromagnetism in a non-dissipative but unknown medium, to back-propagate signals to the sources that emitted them. The initial experiment, see [FWCM91], was to refocus, very precisely, a recorded signal after passing through a barrier consisting of randomly distributed metal rods. Since then, numerous applications of this physical principle have been designed, see [Fin09] or for numerical

---

<sup>1</sup>Bar Ilan University, [franckassous@netscape.net](mailto:franckassous@netscape.net)

<sup>2</sup>University of Paris 6, [nataf@ann.jussieu.fr](mailto:nataf@ann.jussieu.fr), [kray@ann.jussieu.fr](mailto:kray@ann.jussieu.fr)

experiments [LMF<sup>+</sup>06] and references therein. The first mathematical analysis can be found in [BF02] for a homogeneous medium and in [CF97] and [BPZ02] for a random medium. In this study we do not consider random or inhomogeneous media.

This paper is a follow up of [AKNT10, AKNT] in which the *TRAC* (Time-Reversed Absorbing Conditions) method was introduced. This method enables one to “recreate the past” without knowing the location and the properties of the inclusion which diffracted the signals that are back-propagated. This was made possible by removing a small region surrounding the scattering inclusion. This has two applications in inverse problems: the reduction of the size of the computational domain and the determination of the location of an unknown inclusion from boundary measurements. The first application is reminiscent of the redatuming method introduced in [Ber79]. In our case, we use the wave equation and not a paraxial or parabolic approximation. This extends the domain of validity of the redatuming approach. Concerning the second application there is a huge literature that deals with this inverse problem. We mention the MUSIC algorithm [The92] and its application to imaging [LD03], the sampling methods first introduced in [CK96], see the review paper [CCM00] and references therein, and the DORT method [PMSF96]. Mathematical analysis of this kind of approach can be found in [CK98]. These methods were developed in the time-harmonic domain except for the recent work [CHLM10] whereas the *TRAC* method is designed in both the time-dependent and harmonic domains. In the time domain, a well-known technique developed initially for earth imaging, is the reverse time migration *RTM*, [Cla85]. It consists in cross-correlating the incident field with the time reverse scattered field, see right part of figures (6–9).

In this paper we extend the *TRAC* method by considering partial or full aperture for discrete receivers with various spacing. This requires the introduction of two new cost-like functions. Notice that one of them combines the original *TRAC* method with *RTM*, see § 4.1.3. In particular we apply the *TRAC* method to the differentiation between a single inclusion and a two close inclusion case. We stress that in contrast to many inverse problem methods, our method does not rely on any *a priori* knowledge of the physical properties of the inclusion. Hard, soft and penetrable inclusions are treated in the same way. The outline of the paper is as follows. In section 2 we recall the principle of the *TRAC* method for the time dependent wave equation. In section 3, we demonstrate the capacity of the method to recreate the past from boundary measurements in the full or partial aperture case. In section 4, we introduce two new criteria for applying our method to inverse problems. As an illustration, we investigate the ability of the method to differentiate between one inclusion and two close ones. In these numerical examples, the physical parameters are related to iron or plastic mines. We notice that in all our tests, the method has proved to be quite insensitive with respect to noise in the data.

## 2 Principle of the *TRAC* method

In previous papers [AKNT10, AKNT], we introduced a new method that enables one to “recreate the past” without knowing the source which has emitted the signals that will be back-propagated. This was made possible by blending time reversal techniques and absorbing boundary conditions. After removing a small region enclosing the source, we introduced time reversed absorbing conditions (*TRAC*). Let us describe this approach now.

We consider an incident wave  $u^I$  impinging on an inclusion  $D$  characterized by a different propagation speed  $c$  which is constant outside the inclusion  $D$ . The total field  $u^T$  can be

decomposed into the incident and scattered field, so  $u^T := u^I + u^S$ . We consider the problem in  $d$  dimensions  $d = 1, 2, 3$  and assume that the total field satisfies the wave equation

$$\begin{cases} \frac{\partial^2 u^T}{\partial t^2} - c^2 \Delta u^T = 0 \text{ in } \mathbf{R}^d \\ (u^T - u^I)(t, \vec{x}) \text{ satisfies a Sommerfeld condition at } \infty \\ \text{homogeneous initial conditions.} \end{cases} \quad (1)$$

Let  $\Omega$  denote a bounded domain that surrounds  $D$  with  $\Gamma_R$  as its boundary. We assume that the incident wave  $u^I$  is generated by a point source such that after a time  $T_f$  the total field  $u^T$  is negligible in the bounded domain  $\Omega$ . Let  $v$  be a field that satisfies the wave equation.

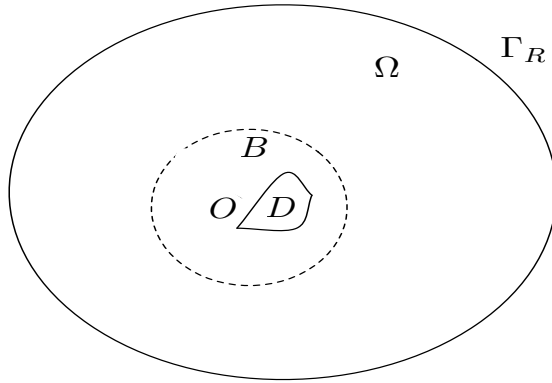


Figure 1: Geometry

We denote by  $v_R$  the corresponding time-reversed field that also satisfies the same physical equation,  $v_R := v(T_f - t, \vec{x})$ . We assume that we have recorded the value of the total field  $u^T$  on the boundary  $\Gamma_R$  that encloses domain  $\Omega$ . Our goal is to derive a boundary value problem (BVP) whose solution is the time-reversed field. The physical properties of the inclusion or the exact location of the body are not known. The only things we know are the physical properties of the surrounding medium, in other words the propagation speed  $c$  outside  $D$ . There  $c$  is assumed to be a constant denoted  $c_0$ . Thus,  $u_R^T$  satisfies the following equation

$$\frac{\partial^2 u_R^T}{\partial t^2} - c_0^2 \Delta u_R^T = 0 \text{ in } (0, T_f) \times \Omega \setminus D. \quad (2)$$

We impose Dirichlet boundary conditions on  $\Gamma_R$  equal to the time-reversal of the recorded fields and zero initial conditions. The key point is that we lack a boundary condition on the boundary of the inclusion in order to define a well-posed BVP on the time-reversed field  $u_R^T$  in  $\Omega \setminus D$ . For inverse problems, the shape and/or location of the inclusion  $D$  is not known and sometimes the type of boundary condition (hard or soft inclusion) on the body is not known either.

To overcome these difficulties, the classical approach for example solves the problem (2) in the entire domain  $\Omega$ , assuming that there is no inclusion  $D$ , see [LMF<sup>+</sup>06] and references therein. Denote by  $w_R^T$  this ‘‘approximate’’ time-reversed solution, we have in the entire domain  $\Omega$ :

$$\frac{\partial^2 w_R^T}{\partial t^2} - c_0^2 \Delta w_R^T = 0 \text{ in } (0, T_f) \times \Omega \quad (3)$$

with Dirichlet boundary conditions on  $\Gamma_R$  equal to the time reversal of the recorded fields and zero initial conditions. One can easily verify that this approximate time-reversed solution  $w_R^T$  differs from  $u_R^T$ .

In [AKNT10, AKNT], we derived a boundary value problem (*BVP*) whose solution is the time-reverse of the scattered field  $u_R^S$ . To derive a boundary value problem satisfied by  $u_R^S$  without knowing the physical properties of the inclusion  $D$  or its exact location, we introduce  $B$  a subdomain enclosing the inclusion  $D$ , see Figure 1. Then, we have to determine a specific boundary condition for  $u_R^S$  on the boundary  $\partial B$  so that the solution to this problem will coincide with  $u_R^S$  in the restricted domain  $\Omega \setminus B$ . In the three space dimension, we introduced the boundary condition named TRAC by

$$\text{TRAC}(u_R^S) := \frac{\partial}{\partial t}(u_R^S(t, \cdot)) + c \frac{\partial}{\partial n}(u_R^S(t, \cdot)) - c \frac{u_R^S(t, \cdot)}{r}. \quad (4)$$

Note, that due to the minus sign before the term  $u_R^S/r$ , the *TRAC* (4) is *not* the  $BT^1$  [BT80] absorbing boundary condition. The time-reversed scattered field  $u_R^S$  satisfies

$$\left\{ \begin{array}{l} \frac{\partial^2 u_R^S}{\partial t^2} - c_0^2 \Delta u_R^S = 0 \text{ in } (0, T_f) \times \Omega \setminus B \\ \text{TRAC}(u_R^S) = 0 \text{ on } \partial B \\ u_R^S(t, \vec{x}) = u^S(T_f - t, \vec{x}) \text{ on } \Gamma_R \\ \text{zero initial conditions.} \end{array} \right. \quad (5)$$

The *TRAC* is not only not the standard  $BT^1$  *ABC* but also has an ‘‘anti absorbing’’ term ( $-cu_R^S/r$ ). A natural concern arises about the well-posedness of *BVP* (5). Although we have not developed a general theory, we prove an energy estimate for this problem in a special geometry, see [AKNT10]. After many computations we have never encountered stability problems. In [AKNT10, AKNT] a numerical procedure for inclusion identification was deduced from this formulation:

*When the subdomain  $B$  encloses the inclusion  $D$  then, the solution in the restricted domain  $\Omega \setminus B$  must be equal to the time reversed solution. Conversely, if the computed solution differs notably from the time reversed solution, it shows that the ball  $B$  does not enclose the inclusion  $D$ .*

The formulation of (4) in two space dimensions is straightforward, see [BT80, BGT82]. In the above formula, it is sufficient to replace  $r$  by  $\sqrt{r}$  and  $1/r$  by  $1/(2r)$  and (4) reads:

$$\frac{\partial u_R^S}{\partial t} + c \frac{\partial u_R^S}{\partial n} - c \frac{u_R^S}{2r} = 0. \quad (6)$$

We have assumed so far, for sake of simplicity, that the surface  $B$  is a sphere or a circle. Since we are finding an approximate location of the inclusion this is usually sufficient. For an elongated body a ball can be replaced by an ellipse or spheroidal surface, see § 4.2. Absorbing boundary conditions for these cases have been developed in [MTH08, MT09, BDSG09]. For more general surfaces several absorbing conditions have been developed, for example [ABB99, KTU87]. Comparison between many options are presented in [MTH08, MT09]. As shown above, a first order *TRAC* method simply reverses the sign of the non-differentiated term of the corresponding first order absorbing boundary condition. Thus, a first order TRAC for a general bounding surface in two dimensions is given by:

$$\text{TRAC}(u_R^S) := \frac{\partial}{\partial t}(u_R^S(t, \cdot)) + c \frac{\partial}{\partial n}(u_R^S(t, \cdot)) - \frac{c\kappa}{2} u_R^S(t, \cdot) \quad (7)$$

where  $\kappa$  is the curvature of the bounding surface  $B$ .

### 3 Recreate the past

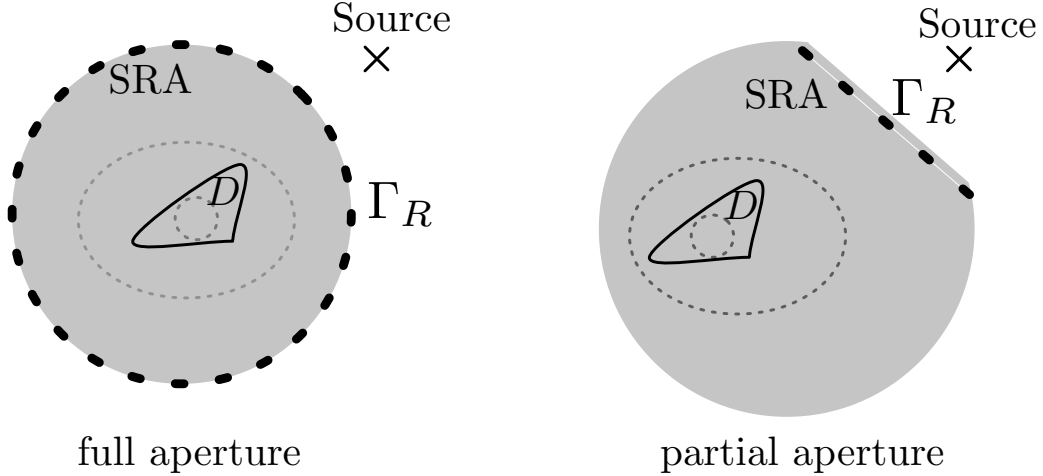


Figure 2: Configurations of the source-receiver array (SRA)

In the proof of concept paper [AKNT10, AKNT], we had already demonstrated the capacity of the TRAC method to recreate the past when the line of receivers  $\Gamma_R$  is continuous and encloses the bounded domain  $\Omega$  as in the geometry shown in figure 1. For a domain  $B$  arbitrary located in  $\Omega$ , we solve the following problem

$$\left\{ \begin{array}{l} \frac{\partial^2 v_R^S}{\partial t^2} - c_0^2 \Delta v_R^S = 0 \text{ in } (0, T_f) \times \Omega \setminus B \\ \text{TRAC}(v_R^S) = 0 \text{ on } \partial B \\ v_R^S(t, \vec{x}) = u^S(T_f - t, \vec{x}) \text{ on } \Gamma_R \\ \text{zero initial conditions,} \end{array} \right. \quad (8)$$

with an *ad hoc* artificial boundary condition on the remaining part of the external boundary. When  $B$  encloses inclusion  $D$ , we know from the previous section that  $v_R^S$  coincides with the restriction of  $u_R^S$  to the domain  $\Omega \setminus B$ . Moreover the method proved to be quite insensitive to the level of noise in the data. Indeed, we added a Gaussian noise by replacing on  $\Gamma_R$  the recorded scattered field  $u^S$  with

$$u^S := (1 + \text{Coeff} * \text{randn}) * u^S, \quad (9)$$

where *randn* satisfies a centered reduced normal law and *Coeff* is the level of noise.

In this paper, in order to be closer to what happens in many real cases as in medical imaging, geophysics, mine detection, ..., we relax these assumptions in two ways:

- we consider a finite number of receivers spaced by a fraction of the central wavelength  $\lambda$ ;
- the aperture is reduced.

In order to create synthetic data, equation (1) is approximated by the FreeFem++ package [Hec10] which implements a finite element method in space. In this study we use a standard  $P^1$  finite element method. The advancement in time is given by a second order central finite difference scheme so that it is time reversible also on the numerical level. The computational domain is a disk and we use an absorbing boundary condition on its external boundary in order to simulate an otherwise infinite domain. We report the results for receivers spaced by  $\lambda/4$  and for both a full aperture and a  $90^\circ$  aperture, see figure 2. In both cases, we consider a soft inclusion in a homogeneous medium with a diameter  $\lambda$ . We first consider a full aperture case. In Fig. 3, we have several lines and five columns. Each column corresponds to a numerical time-reversed experiment and each line corresponds to a snapshot of the solution at a given time, in the domain shaded in figure 2. The top line corresponds to the initial time for the time-reversed problem, equivalent to  $t = T_f$  for the forward problem. The last line is the solution at the final time of the reversed simulation which corresponds to the initial time  $t = 0$  for the forward problem. In column one (namely the left column), we display for reference the perfect time reverse solution which is the reverse of the forward problem.

In columns two and three, we display the solution of the reversed problem (8) with a ball  $B$  which encloses the inclusion. In column two there is no noise in the recorded data on the source-receiver array (SRA) whereas in column three we have 30% noise. As expected, the sequences of snapshots are the restrictions to the domain  $\Omega \setminus B$  of column one. At the expense of removing a domain enclosing the inclusion, we are able to recreate the past even with a high level of noise. This exemplifies an application of the *TRAC* method: when the ball  $B$  encloses the inclusion we are able to reconstruct the signal in a region that is closer to the inclusion than the line of receivers  $\Gamma_R$ . This allows the reduction of the size of the computational domain. In this respect, the method is related to the redatuming method, see [Ber79]. In columns four and five, we show the solutions of the reversed problem (8) with a ball  $B$  smaller than the soft inclusion with no noise and 30% noise respectively. In contrast to the previous cases, the sequence of snapshots differs significantly from column one after the reversed scattered field reached the inclusion. In figure 3, it corresponds to the three last lines.

In the second example we consider a partial aperture problem as depicted in figure 2. Figure 4 is organized the same as the previous one and can be read in the same way. Here again, when the domain  $B$  encloses inclusion  $D$  (columns two and three), we are able to recreate the past but this time only in the cone corresponding to the  $90^\circ$  aperture of the SRA. When the domain  $B$  does not enclose inclusion  $D$  (columns four and five), as in the full aperture case, the sequence of snapshots differs significantly from column one after the reversed scattered field reached the inclusion. Observe that the numerical simulations are quite insensitive to the level of noise.

## 4 Inverse problem

We have seen in the previous section that when the domain  $B$  encloses inclusion  $D$ , the TRAC method is able to recreate the past. But when the domain  $B$  does not enclose inclusion  $D$ , the solution of equation (8) does not coincide with the time reversed scattered field  $u_R^S$ . This property was used in a previous paper [AKNT10, AKNT] to locate the inclusion with a trial and error procedure based on moving the domain  $B$ . Indeed, by playing with the location and size of the subdomain  $B$ , it was possible to determine the location and volume of inclusion  $D$ . The method basically depended on designing a mathematical criterion that tests the computed solution of equation (8) to determine if it corresponds to the time reversed scattered field  $u_R^S$  or not of course without knowing  $u_R^S$ . In the next section, we introduce several criteria to solve the inverse problem.

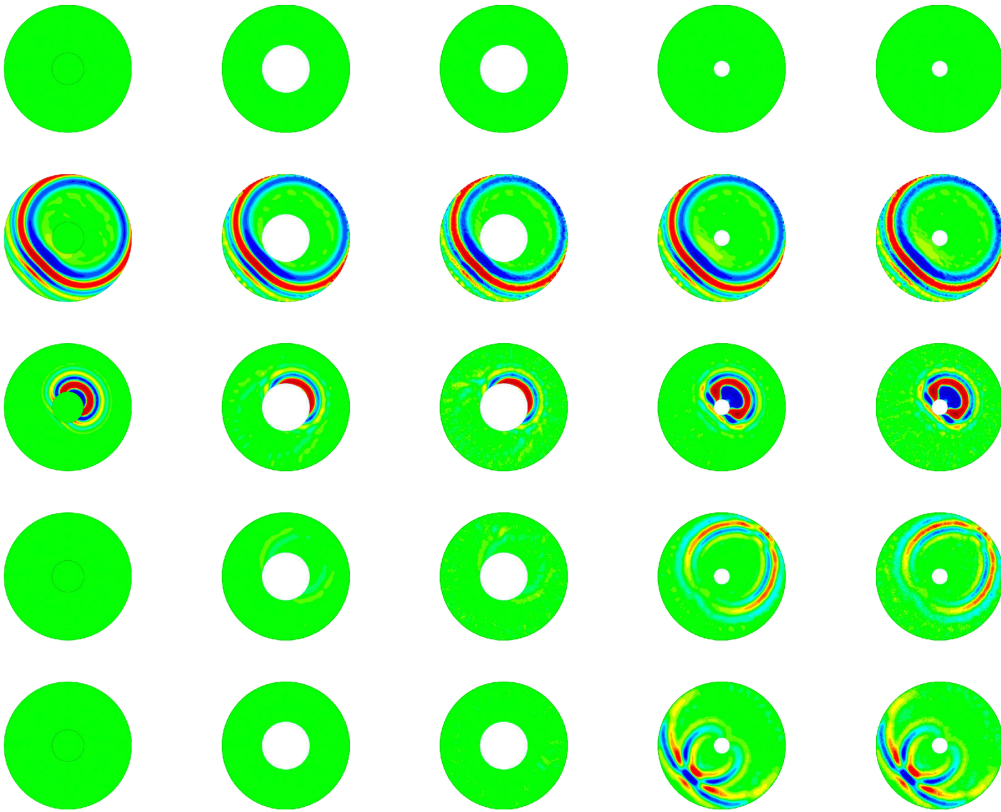


Figure 3: Snapshots for the *TRAC* method in the case of full aperture. Column 1: reverse of the forward problem, columns 2 (no noise) and 3 (30% noise): *TRAC* method when  $D \subset B$ , columns 4 (no noise) and 5 (30% noise): *TRAC* method when  $D \not\subset B$ .

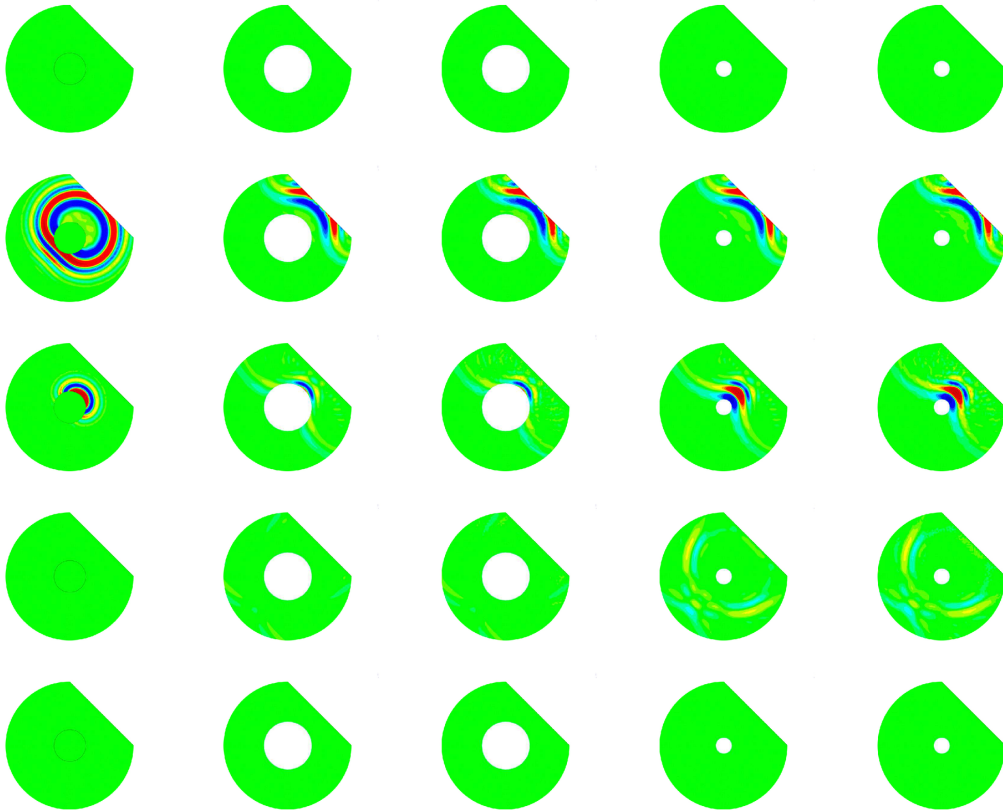


Figure 4: Snapshots for the *TRAC* method in the case of partial aperture. Column 1: reverse of the forward problem, columns 2 (no noise) and 3 (30% noise): *TRAC* method when  $D \subset B$ , columns 4 (no noise) and 5 (30% noise): *TRAC* method when  $D \not\subset B$ .

## 4.1 Criteria

We define three different criteria to assert that the domain  $B$  does not enclose inclusion  $D$ . The first criterion see § 4.1.1 was already introduced in [AKNT10, AKNT]. As we shall see, it works only for the full aperture case. The second and third criteria are effective for partial aperture.

### 4.1.1 Final time criterion

The first criterion named *final time criterion* uses the fact that at the final time the solution should be zero. Conversely, when the final solution is not zero (see columns four and five of figure 3), it proves that  $D$  is not included in domain  $B$ . This observation leads to an easy-to-compute criterion which is independent of the size of the domain:

$$J_{FT}(B) := \frac{\|v_R^S(T_f, \cdot)\|_{L^\infty(\Omega \setminus B)}}{\sup_{t \in [0, T_f]} \|u^I(t, \cdot)\|_{L^\infty(\Omega)}} \quad (10)$$

which vanishes when the artificial domain encloses the inclusion. One could hope that when the criterion is zero, domain  $B$  encloses inclusion  $D$ . Criterion  $J_{FT}$  is normalized w.r.t. the strength of the incident field  $u^I$ . However, the computed reverse time scattered field  $v_R^S$  basically depends on the aperture of the SRA. A full aperture will give a stronger signal than a partial aperture. In order to get comparable figures, for a trial domain  $B$  instead of  $J_{FT}(B)$  defined in (10), we introduce a relative criterion, in the same spirit as the signal-to-noise ratio (SNR),

$$J_{FT}^{rel}(B) := \frac{J_{FT}(\emptyset)}{J_{FT}(B)},$$

where  $J_{FT}(\emptyset)$  is the final time criterion computed in absence of any trial domain  $B$ , the same way as in the classical approach in time reversal techniques. Note that in this case, criterion  $J_{FT}(\emptyset)$  should be large. Consequently, when  $J_{FT}^{rel}(B)$  is close to one, we infer that the domain  $B$  does not enclose the inclusion. In the opposite case, we can reasonably assume that when  $J_{FT}^{rel}(B)$  is large, trial domain  $B$  encloses inclusion  $D$ . As we will see in section 4.2, this is true in practice only for a full aperture case. This motivates the design of two other criteria.

### 4.1.2 Absorbing boundary condition criterion

The second criterion is derived from the use of absorbing boundary conditions. Indeed, the basis of the method is that the time reversed scattered field  $u_R^S$  satisfies

$$\text{TRAC}(u_R^S) = 0 \quad (11)$$

at any point outside the inclusion. In equation (8), this relation is used on the boundary of the artificial domain  $B$  in order to compute  $v_R^S$ . If the domain  $B$  encloses inclusion  $D$ ,  $u_R^S$  and  $v_R^S$  coincide and thus we have, up to approximation errors both in the absorbing condition and in the numerical scheme,

$$\text{TRAC}(v_R^S) = 0 \quad (12)$$

at any point outside the inclusion. Thus, we introduce a new criterion

$$J_{ABC}(B) := \frac{\left\| \left( \frac{\partial}{\partial t} - c_0 \frac{\partial}{\partial r} \right) v_R^S \right\|_{L^\infty((0, T_f) \times \Omega \setminus B)}}{\left\| \left( \frac{\partial}{\partial t} - c_0 \frac{\partial}{\partial r} \right) u^I \right\|_{L^\infty((0, T_f) \times \Omega)}}, \quad (13)$$

where  $r$  is a radial coordinate with the origin at the center of trial domain  $B$ . Since this center is somewhat arbitrary, we have dropped the curvature term which could be too large when the domain  $B$  is small. When trial domain  $B$  encloses inclusion  $D$ , the criterion  $J_{ABC}(B)$  should be small. At the opposite, when part of inclusion  $D$  is outside  $B$ ,  $J_{ABC}$  should be significantly larger. As for the previous criterion, we rather define a relative criterion

$$J_{ABC}^{rel}(B) := \frac{J_{ABC}(\emptyset)}{J_{ABC}(B)},$$

where  $J_{ABC}(\emptyset)$  still denotes the case where there is no trial domain  $B$ . Results are shown in section 4.2.

### 4.1.3 Cross correlation criterion

This criterion is inspired from reverse time migration techniques, [Cla85]. It consists in cross-correlating the incident field  $u^I$  with the time reversed scattered field  $v_R^S$ . In classical applications of earth imaging, the following integral is computed as a function of  $\vec{x} \in \Omega$

$$f(\vec{x}) := \int_{t=0}^{t=T_f} v_R^S(T_f - t, \vec{x}) \times u^I(t, \vec{x}) dt. \quad (14)$$

The function  $f$  images the discontinuities of the propagation speed  $c(\vec{x})$ , see [Cla85]. In this paper, we introduce the following related criterion

$$J_{CC}(B) := \frac{\left\| \int_{t=0}^{t=T_f} v_R^S(T_f - t, \cdot) \times u^I(t, \cdot) dt \right\|_{L^\infty(\Omega \setminus B)}}{\left\| \int_{t=0}^{t=T_f} |u^I(t, \cdot)|^2 dt \right\|_{L^\infty(\Omega)}}, \quad (15)$$

where  $v_R^S$  is the solution to problem. When trial domain  $B$  encloses inclusion  $D$ , there is no discontinuity to be imaged in  $\Omega \setminus B$  and the criterion  $J_{CC}(B)$  should be small. At the opposite, when part of inclusion  $D$  is outside  $B$ , we note that the function  $f$  images this part. So that  $J_{CC}$  should be significantly larger. As for the two previous criteria, we rather define a relative criterion

$$J_{CC}^{rel}(B) := \frac{J_{CC}(\emptyset)}{J_{CC}(B)}, \quad (16)$$

where  $J_{CC}(\emptyset)$  still denotes the case where there is no trial domain  $B$ . Results shown in section 4.2 will prove the robustness and effectiveness of this criterion.

## 4.2 Test cases : numerical results

In section 4.2.1, we validate and compare the three criteria in the case of one inclusion with full or partial aperture with noise in the data. We will see that  $J_{FT}^{rel}$  and  $J_{ABC}^{rel}$  are the criteria of choice for the full aperture case. For a partial aperture, the two other criteria  $J_{ABC}^{rel}$  and  $J_{CC}^{rel}$  are effective. We investigate in § 4.2.2 a more realistic test case with a partial aperture and an unknown number of scatterers. For different geometries of trial domain  $B$ , hard, soft or penetrable inclusions will be studied.

### 4.2.1 One inclusion

We consider a soft inclusion  $D$  and trial domains  $B$  that either enclose or are contained in  $D$  with full or partial aperture as described in section 3. We have four levels of noise from 0% to 30% and various spacings of the receivers from 0 (i.e. a continuous line of receivers) to  $\lambda/2$ ,  $\lambda$  denoting the wavelength of the central frequency of the incident signal. The snapshots are depicted in figures 3 and 4 and the values of the criteria are given in tables 1 and 2.

For a full aperture case, we give in table 1 the values of the three different criteria first when trial domain  $B$  does not enclose inclusion  $D$  (columns three, four and five), then when  $B$  encloses  $D$  (columns six, seven and eight). We recall that the relative criteria close to one aims to indicate that trial domain  $B$  does not enclose inclusion  $D$ . At the opposite, a significant value of the relative criteria should indicate that trial domain  $B$  encloses inclusion  $D$ . In the latter case, the criterion is large but not infinite. This is due to numerical errors and the fact that the *TRAC* is not an exact absorbing boundary condition. In the left part of Table 1 which corresponds to  $D \not\subset B$ , all criteria are close to one and are quite insensitive to the spacing of the SRA or to the level of noise, even for 30% noise. In the right part of Table 1 which corresponds to  $D \subset B$ , the third criteria  $J_{CC}^{rel}$  is not sufficiently discriminating. This is due to the fact that the reverse time migration method which is the basis of the  $J_{CC}^{rel}$  is not a good imaging method in the case of full aperture (contrary to the partial aperture case below). We notice that criteria  $J_{FT}^{rel}$  and  $J_{ABC}^{rel}$  deteriorate with the noise level and the spacing of the SRA. They are discriminating in all cases even for 30% noise.

The corresponding results for a partial aperture case are given in Table 2. Now, the criterion  $J_{FT}^{rel}$  does not work in the sense that in both cases ( $D \not\subset B$  and  $D \subset B$ ) the criterion is close to one. As we see in Figure 4, at the final time of the reverse time simulation, the signal is zero even when domain  $B$  does not enclose inclusion  $D$ . This is due to the use of an artificial boundary condition on the external boundary of the domain not equipped with receivers, see problem (8). This does not occur in the full aperture case where a Dirichlet boundary condition is imposed on this external boundary due to the presence of receivers. Therefore, we will not use the criterion  $J_{FT}^{rel}$  in what follows when we consider only partial aperture examples. The two other criteria  $J_{ABC}^{rel}$  and  $J_{CC}^{rel}$  enable the discriminate between the cases  $D \not\subset B$  and  $D \subset B$ . They are both nearly insensitive to the spacing between the receivers. In addition, the criterion  $J_{CC}^{rel}$  is very effective in this partial aperture case since it is particularly insensitive to noise in the data.

### 4.2.2 One inclusion vs. two inclusions

The aim of this second part is to investigate the ability of the *TRAC* method to discriminate a unique inclusion from two distinct close inclusions. This test is inspired by a more realistic setting. Our intent is to detect one or two iron or plastic mines in a background medium made of sand. The physical equation we use is a scalar wave equation derived from the Maxwell equations, as proposed in [AIL05]

$$\varepsilon \frac{\partial^2 u}{\partial t^2} - \nabla \cdot \left( \frac{1}{\mu} \nabla u \right) = 0, \quad (17)$$

where  $\varepsilon$  denotes the electric permittivity and  $\mu$  the magnetic permeability so that  $\varepsilon \mu c^2 = 1$ . Both of these parameters can be expressed with an absolute value multiplied by a relative value

$$\begin{aligned} \varepsilon &= \varepsilon_0 \varepsilon_r \\ \mu &= \mu_0 \mu_r, \end{aligned}$$

SRA		$D \not\subset B$			$D \subset B$		
Spacing	Noise level	F.T.	A.B.C.	C.C.	F.T.	A.B.C.	C.C.
$\frac{\lambda}{2}$	0%	2.24	1.77	1.27	34.94	10.51	1.75
	10%	2.23	1.79	1.27	21.04	7.72	1.74
	20%	2.24	1.80	1.26	14.73	5.25	1.68
	30%	2.17	1.83	1.26	9.12	3.85	1.63
$\frac{\lambda}{3}$	0%	1.95	1.62	1.42	18.00	10.11	2.67
	10%	1.95	1.60	1.42	16.97	6.55	2.66
	20%	1.95	1.62	1.42	14.34	5.29	2.67
	30%	1.95	1.64	1.41	10.87	3.63	2.52
$\frac{\lambda}{4}$	0%	1.97	1.67	1.46	51.77	9.67	2.94
	10%	1.93	1.64	1.46	40.05	8.30	2.95
	20%	1.98	1.70	1.45	13.50	4.69	2.91
	30%	1.93	1.61	1.42	6.79	4.76	2.95
0	0%	1.84	1.67	1.58	68.25	9.31	3.09
	10%	1.85	1.66	1.58	29.67	7.43	3.09
	20%	1.90	1.77	1.59	13.75	5.75	3.11
	30%	1.75	1.62	1.59	5.06	3.71	3.06

Table 1: Comparison of the three relative criteria for a SRA with a full aperture, in the case of  $D \not\subset B$  and  $D \subset B$ , for different level of noise and different spacing between the receivers in the SRA.

SRA		$D \not\subset B$			$D \subset B$		
Spacing	Noise level	F.T.	A.B.C.	C.C.	F.T.	A.B.C.	C.C.
$\frac{\lambda}{2}$	0%	0.76	2.97	1.07	1.26	5.66	4.99
	10%	1.01	2.89	1.07	1.85	5.20	4.97
	20%	1.15	2.61	1.06	0.90	3.36	4.94
	30%	1.30	2.02	1.06	1.71	2.66	5.44
$\frac{\lambda}{3}$	0%	0.99	2.89	1.01	1.73	11.06	6.88
	10%	1.08	2.73	1.02	1.01	7.21	7.03
	20%	1.78	2.76	1.03	1.55	5.70	7.11
	30%	1.58	2.34	1.02	1.38	4.14	6.71
$\frac{\lambda}{4}$	0%	1.14	2.96	0.98	2.02	13.13	7.40
	10%	1.52	2.62	0.97	1.26	8.38	7.29
	20%	1.77	2.73	0.97	2.09	5.50	7.35
	30%	1.38	2.36	0.99	1.17	4.28	7.62
0	0%	1.16	3.13	0.97	1.90	13.42	7.53
	10%	0.94	2.78	0.98	1.05	10.65	7.50
	20%	0.97	2.98	0.97	1.66	4.92	7.47
	30%	2.62	1.92	0.95	2.95	3.98	7.34

Table 2: Comparison of the three relative criteria for a SRA with a partial aperture, in the case of  $D \not\subset B$  and  $D \subset B$ , for different level of noise and different spacing between the receivers in the SRA.

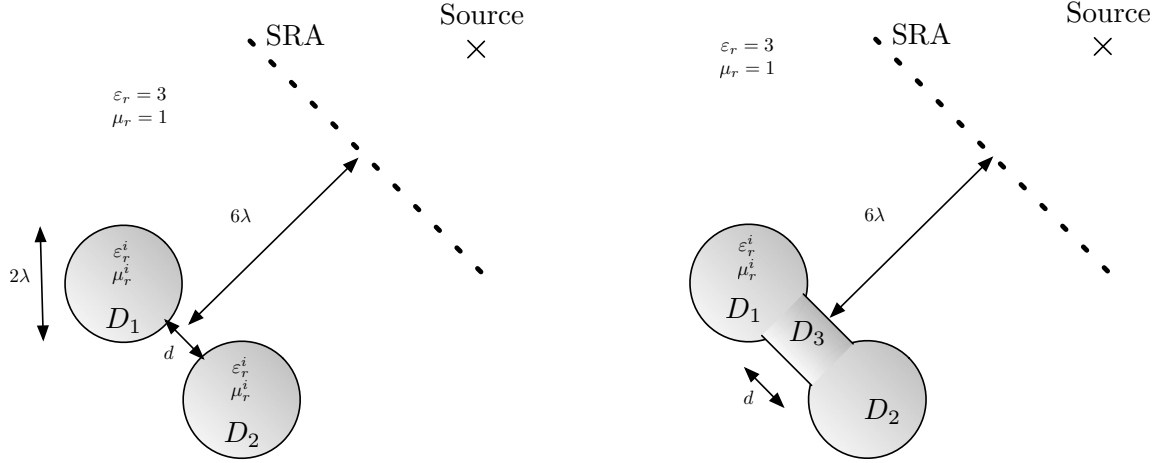


Figure 5: Geometric configuration for two distinct inclusions (left) and a unique inclusion (right). The electromagnetic constants of the inclusion are  $\varepsilon_r^i$  and  $\mu_r^i$ .

where  $\varepsilon_0$  and  $\mu_0$  are the electromagnetic constants of the vacuum

$$\begin{aligned}\varepsilon_0 &= \frac{1}{36\pi} 10^{-9} \text{ F/m} \simeq 8.85 \cdot 10^{-12} \text{ F/m} \\ \mu_0 &= 4\pi 10^{-7} \text{ kg.m/(A.s)}^2 \simeq 12.57 \cdot 10^{-7} \text{ kg.m/(A.s)}^2.\end{aligned}$$

As for the background and the mines, we consider parameters chosen as follows

	sand	iron mine	plastic mine
$\varepsilon_r$	3	1	1.5
$\mu_r$	1	10,000	1

Globally the iron mine acts like a “hard” inclusion, with a velocity ratio

$$\frac{c_{\text{iron}}}{c_{\text{sand}}} = \frac{\frac{1}{\sqrt{10000}}}{\frac{1}{\sqrt{3}}} = \sqrt{\frac{3}{10000}} \sim 0.017 \ll 1,$$

whereas the plastic mines are penetrable inclusions with a ratio velocity close to 1

$$\frac{c_{\text{plastic}}}{c_{\text{sand}}} = \frac{\frac{1}{\sqrt{1.5}}}{\frac{1}{\sqrt{3}}} = \sqrt{\frac{3}{1.5}} = \sqrt{2} \sim 1.41.$$

The geometric configuration is depicted on Figure 5. The source is located at about  $10\lambda$  from the center of the inclusions. Following [FW02], the frequency of the signal is 5 GHz. The length of the SRA is  $5.65\lambda$  and the spacing between the receivers is  $\lambda/4$ , i.e. we have 23 receivers. We study the case of quite far apart inclusions corresponding to  $d = 3\lambda/2$  and close inclusions corresponding to  $d = \lambda/2$ , where  $d$  is the distance between the inclusions. For both iron and plastic mines, we aim to distinguish two inclusions ( $D := D_1 \cup D_2$ ) from one inclusion ( $D := D_1 \cup D_2 \cup D_3$ ), see Figure 5. In the following paragraphs, we first consider iron mines and then plastic mines.

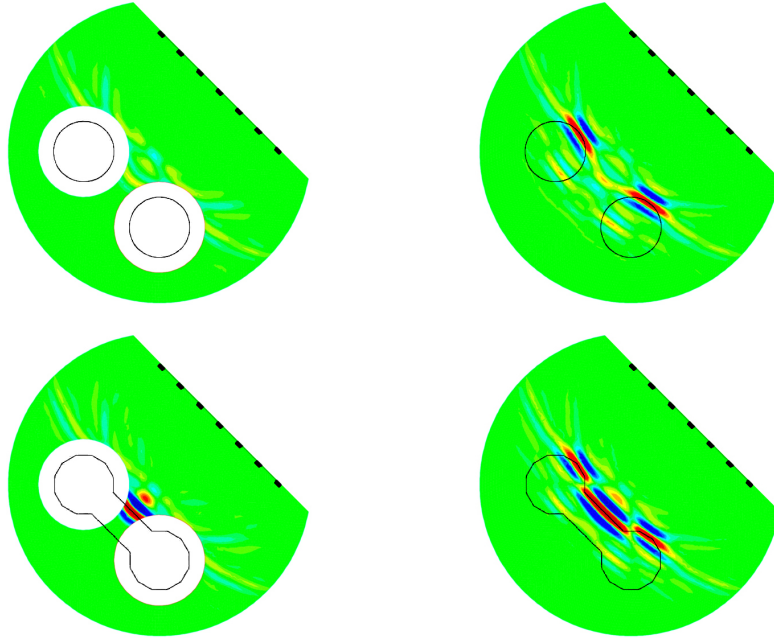


Figure 6: Imaging function (14) for distant iron mines,  $d = 3\lambda/2$ . Left column:  $B$  made of two connected components. Right column:  $B = \emptyset$ .

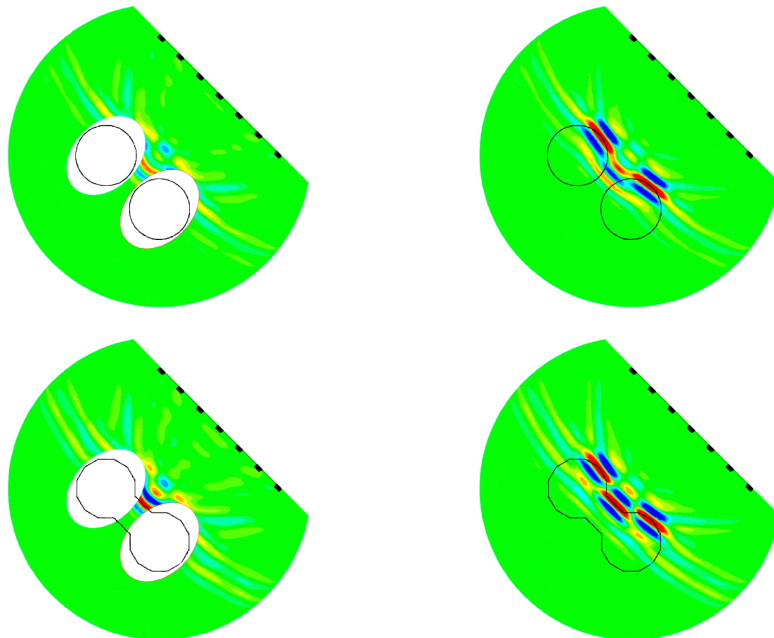


Figure 7: Imaging function (14) for close iron mines,  $d = \lambda/2$ . Left column:  $B$  made of two connected components. Right column:  $B = \emptyset$ .

**Iron mines** On Figure 6, we plot the values of the function  $f$  defined in equation (14) for  $d = 3\lambda/2$ . The first row corresponds to two distinct inclusions whereas the second row deals with a unique inclusion. The right column corresponds to the classical case where  $B = \emptyset$ . In the left column, we use a trial domain  $B$  made of two connected components. When there is no trial domain, the cross-correlation function  $f$  images decently the illuminated edges of the inclusions. Pictures on the left column illustrate the principle of the *TRAC* method. As expected, when trial domain  $B$  encloses the inclusions (top left picture), there is nearly no image. Otherwise, the illuminated edge of the part of the inclusion which is not embedded in  $B$  is correctly imaged (bottom left picture). Thus we are able to distinguish between one inclusion and two close ones, see below a quantitative analysis.

Figure 7 represents the same configuration but for a smaller  $d$  equals to  $\lambda/2$ . When there is no trial domain (right column), the imaging function  $f$  is not able to distinguish two inclusions (top right) from one inclusion (bottom right), due to the proximity of the inclusions. On the contrary when trial domain  $B$  encloses the inclusions (top left), the function  $f$  is significantly smaller than in the case where  $B$  leaves part of the inclusion (part of  $D_3$ ) on the outside (bottom left picture). Note that due to the proximity of the inclusions, we have used trial domains made of two ellipses.

From a more quantitative point of view, we give in Tables 3 and 4 the values of the criteria  $J_{ABC}^{rel}$  and  $J_{CC}^{rel}$  for various levels of noise and trial domains  $B$ . In the first four rows of the tables, trial domain  $B$  is an ellipse that encloses inclusion  $D$ . In the four middle rows of the tables,  $D_2$  is outside trial domain  $B$ . In the last four rows, the trial domain is made of two ellipses that contain respectively the two inclusions  $D_1$  and  $D_2$  but not  $D_3$  in the case of a unique inclusion. In the latter case, we cannot uniquely define an origin to the trial domain. Consequently we cannot use the notion of radial derivative at any point in the computational domain and the criterion  $J_{ABC}$  is not clearly defined. Then, we put crosses in the tables when trial domain  $B$  is not simply connected. As in section 4.2.1, we give the values of the relative criteria  $J_{ABC}^{rel}$  and  $J_{CC}^{rel}$ . Recall that a relative criterion close to one aims to indicate that trial domain  $B$  does not enclose inclusion  $D$ . At the opposite, a significant value of the relative criterion should indicate that trial domain  $B$  encloses inclusion  $D$ . For distant mines (see Table 3), both criteria work as expected, the criterion  $J_{CC}^{rel}$  having the advantage to be reliable in all situations. It asserts that the *TRAC* method is able to distinguish a simply connected inclusion from an inclusion made of two connected components. When the distance  $d$  is smaller ( $d = \lambda/2$ , see Table 4), the results are similar. Nevertheless when the trial domain leaves part of the inclusion outside, the values in the bottom right of Table 4 indicate that it is more difficult but still possible to distinguish one inclusion from two close inclusions.

**Plastic mines** We now consider plastic mines where the reflectivity of the inclusions is small. Figures 8 and 9 are arranged as Figures 6 and 7 respectively. Let us first look at distant mines, see Figure 8. When there is no trial domain, the cross-correlation function  $f$  images decently the edges of the inclusions. The main difference with the iron mines is that the inclusions being penetrable we also image the back part of the inclusions. Pictures on the left column illustrate the principle of the *TRAC* method. When trial domain  $B$  encloses the inclusions (top left picture), there is no significant image. Otherwise, the edges of the part of the inclusion which is not embedded in  $B$  is correctly imaged (bottom left picture). Once again, we are able to distinguish between one inclusion and two close ones. A quantitative analysis will be given in what follows. We now consider the case of close plastic mines, see Figure 9. Due to the proximity of the inclusions, it is difficult to distinguish two inclusions (top right) from one

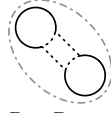
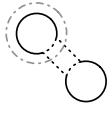
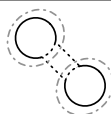
Trial Domain	Noise level	$J_{ABC}^{rel}$		$J_{CC}^{rel}$	
		2 inclusions	1 inclusion	2 inclusions	1 inclusion
 $D \subset B_{\text{ellipse}}$	0%	8.13	11.86	4.78	7.32
	10%	5.89	7.41	4.69	7.35
	20%	5.18	4.86	4.76	7.36
	30%	3.69	3.72	4.62	7.21
 $D_2 \not\subset B$	0%	1.32	1.50	0.96	0.91
	10%	1.30	1.49	0.96	0.91
	20%	1.35	1.46	0.96	0.90
	30%	1.31	1.51	0.96	0.90
 $D_3 \not\subset B$	0%	×	×	5.52	1.07
	10%	×	×	5.48	1.07
	20%	×	×	5.55	1.06
	30%	×	×	5.22	1.06

Table 3: Results of two relative criteria in the case of distant iron mines,  $d = 3\lambda/2$ . Comparison in distinguishing one inclusion from two inclusions.

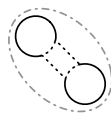
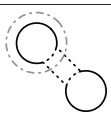
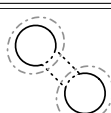
Trial Domain	Noise level	$J_{ABC}^{rel}$		$J_{CC}^{rel}$	
		2 inclusions	1 inclusion	2 inclusions	1 inclusion
 $D \subset B_{\text{ellipse}}$	0%	12.88	13.67	8.13	9.49
	10%	8.48	11.00	8.22	9.49
	20%	6.24	7.88	8.43	9.56
	30%	3.80	4.48	8.33	9.57
 $D_2 \not\subset B$	0%	1.44	1.76	0.92	0.91
	10%	1.41	1.74	0.92	0.91
	20%	1.45	1.76	0.92	0.92
	30%	1.49	1.77	0.91	0.92
 $D_3 \not\subset B$	0%	×	×	3.36	1.55
	10%	×	×	3.33	1.54
	20%	×	×	3.32	1.55
	30%	×	×	3.34	1.56

Table 4: Results of two relative criteria in the case of close iron mines,  $d = \lambda/2$ . Comparison in distinguishing one inclusion from two inclusions.

inclusion (bottom right) in the absence of a trial domain. When trial domain  $B$  encloses the inclusions (top left), function  $f$  is visually smaller than in the case where  $B$  leaves part of the inclusion (part of  $D_3$ ) on the outside (bottom left picture).

As for the values of the criteria, they are given in Tables 5 and 6 that are organized like Tables 3 and 4 respectively. For distant mines (see Table 5), although the inclusions are penetrable, the values are very similar to the case of iron mines. Both criteria work as expected, the criterion  $J_{CC}^{rel}$  still having the advantage of being reliable in all situations. The *TRAC* method is able to distinguish a simply connected penetrable inclusion from one made of two connected components. When the distance  $d$  is smaller ( $d = \lambda/2$ , see Table 6), like for the iron mines it is more difficult but still possible to distinguish one inclusion from two close inclusions.

Note also that in all these numerical experiments, we have used exactly the same methodology for both hard and penetrable inclusions. Moreover, from a quantitative point of view we observe that the values of the criteria are very similar in both cases of iron mines and plastic mines. This is due to our normalization based on the criteria obtained in the absence of a trial domain  $B$ , see formula (16). If one is interested in differentiating iron mines from plastic mines, it is sufficient to consider the non relative criterion  $J_{CC}$ , equation (15). Indeed, the strength of the field scattered by an iron mine is much larger than one scattered by a plastic mine. As an example we report in Table 7 the values of the non relative criterion  $J_{CC}$  in the case of close iron and plastic mines ( $d = \lambda/2$ ) for one or two inclusions. The first four rows correspond to the classical approach  $B = \emptyset$ . One observes a factor of five between the iron and plastic mines for the same geometric configuration.

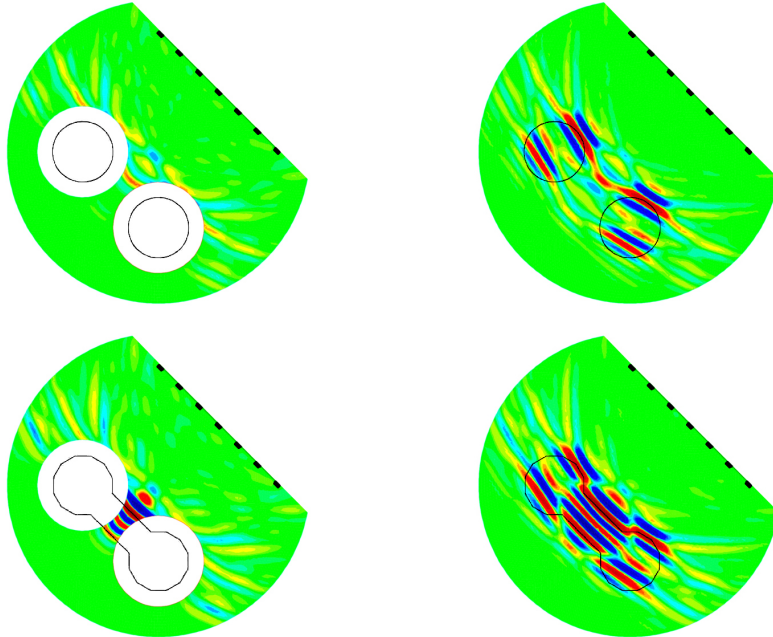


Figure 8: Imaging function (14) for distant plastic mines,  $d = 3\lambda/2$

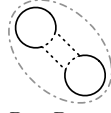
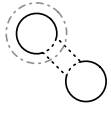
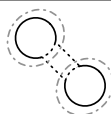
Trial Domain	Noise level	$J_{ABC}^{rel}$		$J_{CC}^{rel}$	
		2 inclusions	1 inclusion	2 inclusions	1 inclusion
 $D \subset B_{\text{ellipse}}$	0%	6.29	10.42	4.68	7.00
	10%	5.58	7.70	4.68	7.04
	20%	4.49	3.41	4.66	7.00
	30%	3.28	3.15	4.77	7.33
 $D_2 \not\subset B$	0%	1.32	1.46	0.94	0.88
	10%	1.32	1.49	0.95	0.88
	20%	1.32	1.45	0.93	0.88
	30%	1.33	1.43	0.94	0.89
 $D_3 \not\subset B$	0%	×	×	4.88	0.92
	10%	×	×	4.89	0.92
	20%	×	×	4.91	0.93
	30%	×	×	4.54	0.92

Table 5: Results of two relative criteria in the case of distant plastic mines,  $d = 3\lambda/2$ . Comparison in distinguishing one inclusion from two inclusions.

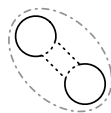
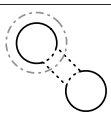
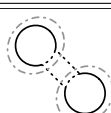
Trial Domain	Noise level	$J_{ABC}^{rel}$		$J_{CC}^{rel}$	
		2 inclusions	1 inclusion	2 inclusions	1 inclusion
 $D \subset B_{\text{ellipse}}$	0%	10.47	11.24	7.82	8.72
	10%	8.61	8.16	7.88	8.63
	20%	4.99	4.58	7.65	8.36
	30%	3.28	3.39	8.09	8.81
 $D_2 \not\subset B$	0%	1.46	1.72	0.98	0.99
	10%	1.42	1.69	0.97	0.99
	20%	1.46	1.73	0.98	0.99
	30%	1.49	1.62	0.98	0.99
 $D_3 \not\subset B$	0%	×	×	3.25	1.70
	10%	×	×	3.20	1.71
	20%	×	×	3.27	1.68
	30%	×	×	3.25	1.69

Table 6: Results of two relative criteria in the case of close plastic mines,  $d = \lambda/2$ . Comparison in distinguishing one inclusion from two inclusions.

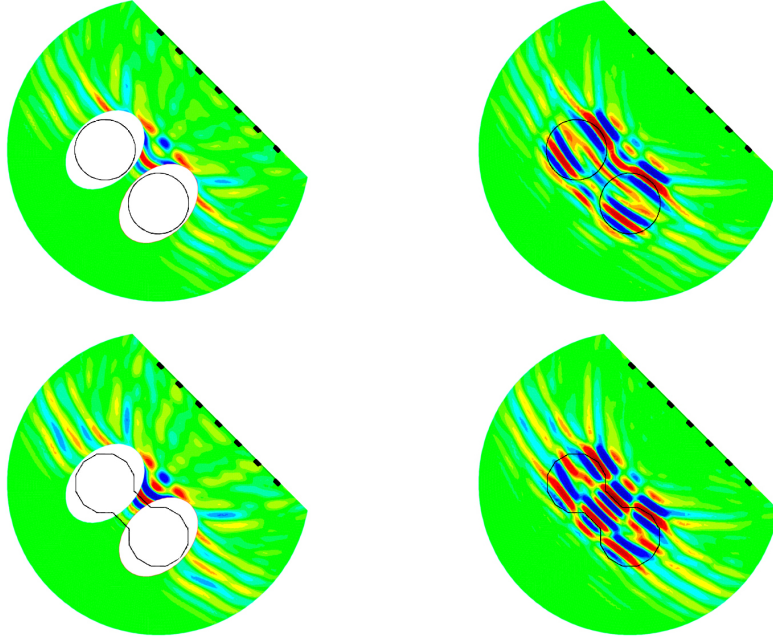


Figure 9: Imaging function (14) for close plastic mines,  $d = \lambda/2$

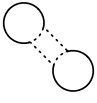
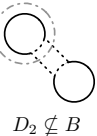
Trial Domain	Noise level	Iron Mines		Plastic Mines	
		2 inclusions	1 inclusion	2 inclusions	1 inclusion
 $B = \emptyset$	0%	31.67	33.24	5.70	6.85
	10%	31.85	33.23	5.68	6.85
	20%	31.70	33.46	5.69	6.83
	30%	31.67	33.50	5.65	6.82
 $D \subset B_{\text{ellipse}}$	0%	3.89	3.50	0.73	0.79
	10%	3.87	3.50	0.72	0.79
	20%	3.76	3.50	0.74	0.82
	30%	3.80	3.50	0.70	0.77
 $D_2 \not\subset B$	0%	34.41	36.42	5.80	6.94
	10%	34.50	36.42	5.83	6.90
	20%	34.45	36.42	5.79	6.90
	30%	34.88	36.42	5.76	6.89
 $D_3 \not\subset B$	0%	9.44	21.49	1.75	4.03
	10%	9.56	21.52	1.77	4.01
	20%	9.55	21.55	1.74	4.07
	30%	9.47	21.42	1.74	4.03

Table 7: Non relative criterion  $J_{CC}$  (equation (15)) for close iron vs. plastic mines. Comparison in distinguishing one inclusion from two inclusions for various trial domains.

## 5 Conclusion

This paper is a follow up of [AKNT10, AKNT] in which was introduced the *TRAC* (Time-Reversed Absorbing Conditions) method. It enables one to “recreate the past” without knowing

the location and the properties of the inclusion which diffracted the signals that are back-propagated. This was made possible by removing a small region surrounding the scattering inclusion. This has two applications in inverse problems: the reduction of the size of the computational domain and the determination of the location of an unknown inclusion from boundary measurements. In this paper we extend the method by considering partial or full aperture for discrete receivers with various spacing. This requires the introduction of two new criteria  $J_{ABC}$  and  $J_{CC}$ . In particular we apply the *TRAC* method to the differentiation between one inclusion and two close ones. We stress that in contrast to many methods in inverse problems, our method does not rely on any *a priori* knowledge of the physical properties of the inclusion. Hard, soft and penetrable inclusions are treated in the same way. Moreover, the method has proved to be quite insensitive with respect to noise in the data.

## References

- [ABB99] Xavier Antoine, Helene Barucq, and A. Bendali. Bayliss-turkel like radiation conditions on surfaces of arbitrary shape. *J. Math. Anal. Appl.*, 229:184–211, 1999.
- [AIL05] Habib Ammari, Ekaterina Iakovleva, and Dominique Lesselier. A MUSIC algorithm for locating small inclusions buried in a half-space from the scattering amplitude at a fixed frequency. *Multiscale Modeling and Simulation*, 3(3):597–628, 2005.
- [AKNT] F. Assous, M. Kray, F. Nataf, and E. Turkel. Time reversed absorbing condition: Application to inverse problem. <http://hal.archives-ouvertes.fr/hal-00491912/fr/>.
- [AKNT10] F. Assous, M. Kray, F. Nataf, and E. Turkel. Time reversed absorbing condition. *CR. Acad. Sci. Paris, Ser. I*, 2010. doi:10.1016/j.crma.2010.09.014.
- [BDSG09] Helene Barucq, Rabia Djellouli, and A. Saint-Guirons. Performance assessment of a new class of local absorbing boundary conditions for elliptical- and prolate spheroidal-shaped boundaries. *Appl. Numer. Anal.*, 59:1467–1498, 2009.
- [Ber79] J.R. Berryhill. Wave-equation datuming. *Geophysics*, 44(206):132944, 1979.
- [BF02] Claude Bardos and Mathias Fink. Mathematical foundations of the time reversal mirror. *Asymptot. Anal.*, 29(2):157–182, 2002.
- [BGT82] Alvin Bayliss, Max Gunzburger, and Eli Turkel. Boundary conditions for the numerical solution of elliptic equations in exterior regions. *SIAM J. Appl. Math.*, 42(2):430–451, 1982.
- [BPZ02] P. Blomgren, G. Papanicolaou, and H. Zhao. Super-resolution in time-reversal acoustics. *J. Acoust. Soc. Am.*, 111:230–248, 2002.
- [BT80] A. Bayliss and E. Turkel. Radiation boundary conditions for wave-like equations. *Comm. Pure Appl. Math.*, 33(6):707–725, 1980.
- [CCM00] David Colton, Joe Coyle, and Peter Monk. Recent developments in inverse acoustic scattering theory. *SIAM Rev.*, 42(3):369–414 (electronic), 2000.
- [CF97] J. F. Clouet and J. P. Fouque. A time-reversal method for an acoustical pulse propagating in randomly layered media. *Wave Motion*, 25(4):361–368, 1997.

- [CHLM10] Q Chen, H Haddar, A Lechleiter, and P Monk. A sampling method for inverse scattering in the time domain. *Inverse Problems*, 26(8):085001, 2010.
- [CK96] David Colton and Andreas Kirsch. A simple method for solving inverse scattering problems in the resonance region. *Inverse Problems*, 12(4):383–393, 1996.
- [CK98] David Colton and Rainer Kress. *Inverse acoustic and electromagnetic scattering theory*, volume 93 of *Applied Mathematical Sciences*. Springer-Verlag, Berlin, second edition, 1998.
- [Cla85] Jon F. Claerbout. *Imaging the Earth’s interior*. Blackwell, 1985.
- [Fin09] M. Fink. *Renversement du temps, ondes et innovation*. Ed. Fayard, 2009.
- [FW02] Christian Fischer and Werner Wiesbeck. Multistatic antenna configurations and image processing for mine-detection GPR. [www.hdic.jmu.edu/dtif/Conferences/Ispra2/papers/fischer.pdf](http://www.hdic.jmu.edu/dtif/Conferences/Ispra2/papers/fischer.pdf), 2002.
- [FWCM91] M. Fink, F. Wu, D. Cassereau, and R. Mallart. Imaging through inhomogeneous media using time reversal mirrors. *Ultrasonic Imaging*, 13(2):199 – 199, 1991.
- [Hec10] Frédéric Hecht. *FreeFem++*. Numerical Mathematics and Scientific Computation. Laboratoire J.L. Lions, Université Pierre et Marie Curie, <http://www.freefem.org/ff++/>, 3.7 edition, 2010.
- [KTU87] Gregory Kriegsmann, Allen Taflove, and K.R. Umashankar. A new formulation of electromagnetic scattering using on surface radiation condition approach. *IEEE Trans. Ant. Prop.*, AP35:153–161, 1987.
- [LD03] Sean K. Lehman and Anthony J. Devaney. Transmission mode time-reversal super-resolution imaging. *J. Acoust. Soc. Am.*, 113 2742, 2003.
- [LMF<sup>+</sup>06] C. Larmat, J.-P. Montagner, M. Fink, Y. Capdeville, A. Tourin, and E. Clévéde. Time-reversal imaging of seismic sources and application to the great sumatra earthquake. *Geophys. Res. Lett.*, 33, 2006.
- [MT09] Michael Medvinsky and Eli Turkel. On surface radiation conditions for an ellipse. *JCAM*, 234:1647–1655, 2009.
- [MTH08] Michael Medvinsky, Eli Turkel, and Ulrich Hetmaniuk. Local absorbing boundary conditions for elliptical shaped boundaries. *J. Comput. Phys.*, 227(18):8254–8267, 2008.
- [PMSF96] C. Prada, S. Manneville, D. Spoliansky, and M. Fink. Decomposition of the time reversal operator: Application to detection and selective focusing on two scatterers. *J. Acoust. Soc. Am.*, 99 (4):2067–2076, 1996.
- [The92] C. W. Therrien. *Discrete Random Signals and Statistical Signal Processing*. Englewood Cliffs, NJ: Prentice- Hall, 1992.